

This is an Open Access document downloaded from ORCA, Cardiff University's institutional repository:<https://orca.cardiff.ac.uk/id/eprint/69906/>

This is the author's version of a work that was submitted to / accepted for publication.

Citation for final published version:

Lamour, Sabrina D., Veselkov, Kirill A., Posma, Joram M., Giraud, Emilie, Rogers, Matthew E., Croft, Simon, Marchesi, Julian Roberto, Holmes, Elaine, Seifert, Karin and Saric, Jasmina 2015. Metabolic, immune, and gut microbial signals mount a systems response to *Leishmania major* infection. *Journal of Proteome Research* 14 (1), pp. 318-329. 10.1021/pr5008202

Publishers page: <http://dx.doi.org/10.1021/pr5008202>

Please note:

Changes made as a result of publishing processes such as copy-editing, formatting and page numbers may not be reflected in this version. For the definitive version of this publication, please refer to the published source. You are advised to consult the publisher's version if you wish to cite this paper.

This version is being made available in accordance with publisher policies. See <http://orca.cf.ac.uk/policies.html> for usage policies. Copyright and moral rights for publications made available in ORCA are retained by the copyright holders.



Metabolic, immune, and gut microbial signals mount a systems response to *Leishmania major* infection

*Sabrina D. Lamour[†], Kirill A. Veselkov[†], Joram M. Posma[†], Emilie Giraud[‡], Matthew E. Rogers[§],
Simon Croft[‡], Julian R. Marchesi^{#||}, Elaine Holmes[†], Karin Seifert[‡], and Jasmina Saric^{†*}*

[†] Division of Computational and Systems Medicine, Department of Surgery and Cancer, Imperial College London, London, SW7 2AZ, UK

[‡] Department of Immunology and Infection, London School of Hygiene & Tropical Medicine, London, WC1E 7HT, UK

[§] Department of Disease Control, London School of Hygiene & Tropical Medicine, London, WC1E 7HT, UK

[#] Cardiff School of Biosciences, Division of Microbiology, Cardiff University, Cardiff, CF10 3AT, UK

^{||} Centre for Digestive and Gut Health, Imperial College London, London, SW7 2AZ, UK

* Correspondence should be addressed to: Dr Jasmina Saric, Division of Computational and Systems Medicine, Department of Surgery and Cancer, Imperial College London, Sir Alexander Fleming Building, South Kensington, London SW7 2AZ, United Kingdom. Tel.: +44 20 7594-3899; E-mail: jasmina.saric@imperial.ac.uk

RUNNING TITLE: Systemic host responses to *Leishmania* infection

KEYWORDS: host, response, infection, metabolic, profiling, microbiota, cytokine, multivariate, correlation, Leishmania

ABSTRACT

Parasitic infections such as *Leishmania* induce a cascade of host physiological responses, including metabolic and immunological changes. Infection with *Leishmania major* protozoa causes cutaneous leishmaniasis in humans, a neglected tropical disease with suboptimal disease management. To understand the determinants of pathology, we studied *L. major* infection in two mouse models: the self-healing C57BL/6 strain and the non-healing BALB/c strain. Metabolic profiling of urine, plasma and faeces *via* proton NMR spectroscopy was performed, a method that has shown great promise in discovering parasite-specific imprints on global host metabolism. Plasma cytokine status and faecal microbiome were also characterised, as additional metrics of the host response to infection. Results demonstrated differences in glucose and lipid metabolism, distinctive immunological phenotypes, and shifts in microbial composition between the two models. We present a novel approach to integrate such metrics using correlation network analyses, whereby self-healing mice demonstrated an orchestrated interaction between the biological measures shortly after infection. In contrast, the response observed in non-healing mice was delayed and fragmented. Our study suggests that trans-system communication across host metabolism, the innate immune system and gut microbiome is key for a successful host response to *L. major* and provides a new concept, potentially translatable to other diseases.

INTRODUCTION

The leishmaniasis describe a spectrum of diseases that are caused by protozoan parasites of the genus *Leishmania*. The sum of diseases results in significant health burden globally, estimated at approximately 2.4 million DALY's^{1,2}. There are severe limitations to the current management of these, including variable clinical manifestations and severity of disease (including the cutaneous and visceral forms), suboptimal diagnosis, limited treatments and increases in drug resistance.³ A more fundamental understanding of the pathogenesis is thus key to progressing novel avenues for more effective identification and treatment.

Experimental research on murine models for cutaneous leishmaniasis (CL) has shown that disease outcome depends to a large extent on the immune-phenotype of the host. A dominant Th1 response, prevalent in C57BL/6 mice, with marked increased IFN γ and IL-12 cytokine production, has been associated with disease resolution.^{4,5} In contrast, a dominant Th2 response with elevated IL-4 levels, as observed in BALB/c mice, has been linked with disease progression.^{6,7}

Recent evidence has shown that a range of different leukocytes, including different Th subsets, and signalling molecules significantly contribute to the host response to *Leishmania* infection.⁸⁻¹⁰ Furthermore, host defence to *Leishmania* is not solely built on immune components but also relies on regulatory metabolic messengers, such as the arginine pathway intermediates.^{11,12} This special liaison between immune and metabolic system has only found attention in the last few years and hence still represents a largely unexplored source of potential new information on infection mechanisms.¹³⁻¹⁵

Metabolic profiling has shown great promise in discovering parasite-specific imprints on global host metabolism but has not yet been investigated with *Leishmania* infection *in vivo*. Such studies on other parasitic infections have conventionally relied on ¹H nuclear magnetic resonance (NMR) spectroscopy-based screening of urine and plasma samples, taken from infected rodent hosts for diagnostic

biomarker research.^{16, 17} NMR-based analyses, combined with advances in multivariate statistical tools, have shown to yield highly reproducible data, with correlation of variances (CV's) of major metabolite markers typically below 10%.^{18, 19} This approach in infection studies has expanded successively to include tissues and, more recently, to combine metrics from both the metabolic and immune system. Such a combined approach enables a more systemic view on host response to a pathogen and characterises the immune–metabolic interface during infection.²⁰

A recurrent theme across a range of these parasite–rodent models characterised by metabolic profiling is the association between parasitic infection and an altered host microbiome, as indicated by a set of microbiota-associated metabolites detected in the urine and plasma.^{16, 17, 21} Additionally, results from *L. major* infection models have demonstrated that germ-free mice failed to heal lesions as compared with their conventional counterparts, despite generating a strong Th1 immune response²², which strongly implicates the microbiota in mounting a successful host response to the parasite.

The current study was performed to characterise the infection-specific response in a self-healing C57BL/6 and a non-healing BALB/c experimental model for CL (Figure 1). We adopted a holistic approach to investigate the early phase of *L. major* infection by combining metrics of the immune, metabolic, and gut microbial response in the host, including metabolic profiles from urine, plasma, and faeces, selected peripheral cytokines, and faecal bacterial composition. By using this combined set of phenotypic metrics, we aim to gain a better understanding of the interactions that lead to the complex pathology of leishmaniasis. Moreover, by taking the successfully resistant mouse phenotype as a reference system, we intend to define those biological parameters of the host that are associated with disease resolution.

MATERIALS AND METHODS

Ethics Statement

All animal experiments were performed at Imperial College London, adhering to local and national animal handling guidelines, under project license PPL70/6997. The protocols were approved by the animal ethics committees at London School of Hygiene & Tropical Medicine, Imperial College London and the UK Home Office.

Experimental Model and Sample Collection

L. major infection was established in 7-8 week old female C57BL/6J mice and BALB/cJ mice ($n=15$ per strain, 10 infected and 5 controls), purchased from Charles River Ltd, UK. Mice were fed on standard rodent diet (Rat and Mouse No. 1 Maintenance diet, Special Diets Service, UK). Following one week acclimatisation, mice were randomly allocated into infection and control groups. Mice in the infection group received subcutaneous (s.c.) injections with 2×10^6 stationary phase *L. major* promastigotes (strain MHOM/SA/85/JISH118, passage 2 — culture methods detailed in Supporting Information) in 100 μ l Schneider's Insect Medium (Sigma-Aldrich) into the shaven rump, whereas the control group received medium only. Plasma, urine, and faecal samples were taken from each mouse 2 days prior to infection and post-infection at days 2, 6, and at the terminal day of the study, defined as the day the lesion had developed in the tail before ulceration occurred (7-13 days post-infection, depending on each infected animal), or 12 days post-injection for control animals. Samples were snap frozen in liquid nitrogen and stored at -40°C for metabolic analysis. Additional faecal pellets for microbial assessment were taken at all four time-points, as well as extra sections of terminal day lesion (or skin for controls) for measurement of parasitic burden, which were all fixed in 10% formalin and subsequently stored at -20°C .

^1H NMR Acquisition and Processing

Plasma, urine and faecal samples were prepared for ^1H NMR analyses based on protocols as described by Beckonert *et al.*, 2007²³, where methods for tissue metabolite extraction were adjusted for preparation of faeces (Supporting Information). ^1H NMR data were acquired on a Bruker Avance 600 NMR Spectrometer with TXI probe head (Bruker), using XWIN-NMR software (Bruker BioSpin). Acquisition settings are outlined in Supporting Information. Spectra were pre-processed using automatic phasing, baseline correction and reference peak calibration *via* an in-house algorithm in MATLAB (version R2012b, Mathworks Inc) and Topspin 3.1 software (Bruker BioSpin). Water (and urea regions for urine) were removed prior to automatic spectral alignment and probabilistic quotient normalisation²⁴, using an in-house MATLAB script.

Plasma Cytokine Assessment

Following NMR acquisition, plasma samples were tested in duplicate *via* the ultra-sensitive plasma Th1/Th2 Cytokine 9-plex assay kit (Meso Scale Discovery/MSD) for levels of IFN γ , IL-1 β , IL-2, IL-4, IL-5, CXCL1, IL-10, IL-12 and TNF α . Protocols were based on manufacturer's instructions, with sample incubation time increased to 3 hours for increased detection. Assay plates were read on Sector Imager 2400 and concentrations calculated using accompanying Discovery Workbench MSD software.

Faecal Microbiota Diversity Analysis with next-generation sequencing

Faecal DNA was extracted using QIAmp Stool Mini Kit (QIAGEN) based on manufacturer's instructions with minor protocol amendments (Supporting Information). Presence of microbial genes was confirmed *via* 35 cycles of PCR [30 sec at 95°C, 40 sec at 55°C, 60 sec at 72°C], using primers against V1-V3 region of bacterial 16S rRNA genes as described by Lewis *et al.*, 2013.²⁵ DNA samples were sequenced *via* next-generation pyrosequencing using a 454 FLX Genome Sequencer (Roche) by Research and Testing Laboratory, LLC (Texas, USA), and data was processed and analysed according to company guidelines. In order to be able to discriminate between functionally distinctive groups of

bacteria, as opposed to purely genotypic differences when assessing changes at lower taxonomic levels, the presented data was analysed at the class level, comparing relative percentage abundance of bacteria between samples. Top eight bacterial classes with highest abundance were used for final analyses, representing 99.1% of all measured classes across the dataset.

Parasitic Burden Assessment *via* real-time PCR

DNA was extracted from lesion samples using DNeasy® Blood & Tissue Kit (QIAGEN), following manufacturer's instructions, with minor modifications (PBS wash steps before extraction and doubling proteinase K for lesion samples). DNA concentration and purity was measured using Nanodrop® (Thermo Scientific). Real-time PCR was performed with triplicate samples using SYBR-Green kit (Applied BioSystems)²⁶ and primers against mouse arginase 1, to quantify genomic DNA, and *Leishmania*-specific RV1/RV2²⁷ to detect parasites. Parasitic burden for each sample was assigned as average fluorescent intensity of parasitic DNA as a multiple of the lowest positive reading, normalised to arginase levels and calculated with Qbase Plus 2.4 software (Biogazelle).

Statistical Analysis and Data Integration

Metabolic spectra of infected and control groups from both strains were initially analysed by Principal Component Analysis (PCA).²⁸ Graphical representations of the first several components were used to explore overall similarities/differences in metabolic phenotypes, using SIMCA P+ software (V. 12.0, Umetrics). Mouse strain differences at the pre-infection time-point, as well as infection-associated differences between infected and time-matched control mice for each strain were then explored using Orthogonal Partial Least Squares Discriminatory Analysis (O-PLS-DA)²⁹ which includes a 7-fold cross validation for each biological matrix, at each time-point. Final analyses focused on the comparison between the infection-related responses of the two mouse models, whereby to account for the strain differences, metabolic spectra, cytokine, and microbiome datasets from infected mice were

adjusted to their respective control strain by subtracting the uninfected control group median spectra level from infected data. The strain-adjusted metabolic data was further analysed *via* O-PLS-DA. Assigned discriminatory metabolites from O-PLS-DA models were selected when the associated Pearson-product moment correlation coefficient (r) of a given metabolite peak surpassed the critical values for $p < 0.05$ and its ROC sensitivity/specificity score was at least 0.8. Spectral assignments of metabolite peaks were performed based on Chenomx NMR suite profiler 7.0 software and using known assignments from in-house NMR databases and literature.²¹

The differences in individual cytokines and class microbiota levels were analysed using non-parametric univariate tests: Kruskal-Wallis ANOVA and pair-wise Mann-Whitney U-test for time-matched strain comparisons, and Friedman tests and Wilcoxon matched-pair tests, for comparative analyses between time-points for each mouse model. Bonferroni correction was applied to account for multiple testing. Baseline plasma samples from the control groups were lacking thus no control-strain adjustment could be performed for plasma metabolic and cytokine data at this time-point, required for spectral O-PLS-DA and cytokine univariate analyses, respectively.

Two-dimensional-matrix, Pearson-based, correlation analyses were performed between time-matched spectral data and cytokine levels, spectral data and microbiota class percentages, and cytokine levels and microbiota, using in-house MATLAB code (Dr Judith Fonville). The script included a 10,000-fold random permutation of sample order. A p -value was calculated as the number of times the absolute value of correlation coefficient of the re-sampled data exceeded the original correlation coefficient value. Only correlative pairs with $p < 0.05$ were displayed. Twelve metabolites were selected each from urine, plasma, and faeces, based on their display of correlations with host cytokines and/or microbiome, and on their discriminatory role in differentiating between the two CL mouse models. The integrals were calculated and co-analysed alongside time-matched microbiota class percentage abundance and

cytokine levels *via* PCA and PLS-DA, to determine how the different datasets (48 variables in total) drive the separation between the two infection models.

These same variables were correlated *via* Pearson correlation with relative levels of parasitic burden for each mouse model, to determine direct associations between infection and host measures. Furthermore, Pearson correlation network graphs were drawn for each time-point in both strains individually, to determine specific host interactions between variables, in response to infection, using in-house MATLAB code based on MetaboNetworks software.³⁰ A generous cut-off for the q-values of 0.3 using the Storey-Tibshirani False Discovery Rate³¹ was applied for multiple testing correction in the parasite–host correlation as well as correlation network analyses, for maximal exploration of potential biologically relevant host interactions in this study. The sample size of this study was small and future studies are needed to perform targeted analyses to test these associations. The majority of associations are still expected to be true discoveries.

RESULTS

BALB/c and C57BL/6 mice have different metabolic, immune, and gut microbial phenotypes in response to *L. major* infection

Among the physiological and pathological measures that were monitored between the two strains within the first two weeks of infection, only the haematocrit differed significantly (Table S1). No significant changes were observed in weight, day of lesion onset, or lesion size (though trends showed that the BALB/c had larger overall lesions). Infection with *L. major* was confirmed *via* real-time PCR of *L. major* DNA in lesions taken at the terminal time-point (days 7-13 post infection, the most acute phase of the infection in our study), with no significant differences observed between strains.

In contrast to the minor pathological changes, the strains displayed clear strain and infection-related differences in their metabolism across the three assessed biofluids: urine, plasma, and faecal extracts. Preliminary multivariate analyses using PCA and O-PLS-DA revealed that strain differences prior to infection included significantly higher levels of glucose and lactate with lower lipid moieties, in plasma of C57BL/6 mice compared with BALB/c. The latter strain also displayed relatively higher lipid levels in their faeces, along with lower amounts of urinary citrate, succinate and 2-oxoadipate. Infection resulted in significant decreases in plasma glucose and urinary hippurate across both strains, as well as decreases in plasma lipids in non-healing BALB/c mice. To investigate the differences in metabolic infection-related responses between the two models, finalised results (Table S2) were based on O-PLS-DA on spectra that took into account strain differences unrelated to infection by adjusting each infected group to their respective uninfected control strain, a method that was also applied to subsequent cytokine and microbiome data (Materials and Methods). Metabolites with significantly higher levels in the non-healing strain for at least one post-infection time-point included alanine (in plasma and faeces), succinate (faeces), 3-hydroxybutyrate (3-HB) and glucose (in plasma), as well as the gut-microbiota-associated metabolites phenylacetylglcine (PAG) and trimethylamine (TMA) in the urine. In contrast,

metabolites found in higher concentrations in the self-healing strain after infection included urinary acetate and several fatty acid moieties from lipoproteins in plasma.

Out of the nine cytokines initially tested in plasma, four displayed detectable levels, namely IL-1 β , IL-10, IL-12 and CXCL1. IL-1 β was the only cytokine to be significantly different between the two strains prior to infection (higher in BALB/c mice, $p=0.006$). Following strain adjustment, infection-related differences between the models (Figure S1) showed that non-healing mice generally had higher levels of the pro-inflammatory cytokines CXCL1 and IL-1 β than the self-healing model over all time-points, though reaching statistical significance only for IL-1 β , 6 days post-infection (d 6 p.i., $p=0.036$). They also had higher levels of cytokine IL-12 than self-healing mice, 2 days post infection (d 2 p.i., $p=0.013$).

To compare faecal microbial composition between animals, we assessed changes in percentage abundance of bacterial classes (further outlined in Materials and Methods). *Clostridia* (phylum *Firmicutes*) and *Gammaproteobacteria* (phylum *Proteobacteria*) were the most dominant classes of faecal bacteria observed in this study across both strains, accounting for over 85% relative abundance of the total data. Initial trends showed that *Clostridia* were higher in BALB/c mice whilst *Gammaproteobacteria* were higher in C57BL/6 mice before infection, yet this was not significant. Following strain-adjustment, infection-related microbial levels for *Clostridia* remained consistently higher in the BALB/c strain, reaching significance at the terminal time-point ($p=0.003$, Figure 2A). A considerable decrease in relative *Gammaproteobacteria* levels was observed in both strains by the end of the study (significant in C57BL/6 mice, $p=0.048$), although levels in C57BL/6 mice remained significantly higher than in BALB/c mice ($p=0.006$, Figure 2B).

Erysipelotrichia represented the third most abundant bacterial class, which was largely absent in BALB/c mice and, where present, was significantly lower than in self-healing C57BL/6 mice, d 6 p.i. ($p=0.013$; Figure 2C, Table S3). The remaining bacterial classes were only detected at low levels

(typically less than 5% relative abundance), although significant changes relative to baseline were detected in self-healing mice, e.g. increases in *Alphaproteobacteria* (d 2 p.i., $p=0.048$) and *Bacteroidia* (d 2 p.i., $p=0.012$ and terminal, $p=0.048$) and decreases in *Actinobacteria* (d 6 p.i., $p=0.027$) and *Bacilli* (terminal day, $p=0.048$; Table S4). No significant changes in faecal bacterial composition were evident over the study period in non-healing mice, indicating a more static microbial population than that observed in the self-healing model (Tables S3 and S4).

Peripheral cytokines correlate with the systemic host metabolism

Correlation analysis was performed between cytokine and NMR spectral data, in order to identify associations between the host immune and metabolic system in response to infection, for each of the murine phenotypes. Results showed that multiple interactions existed between the cytokine and the metabolite data for all three biofluids (Table 1), with a higher number of correlations determined in the self-healing strain. Certain immune-metabolic correlates were common to both the self-healing and non-healing models, e.g. a negative association between urinary hippurate and IL-10. Other correlations were specific to a particular CL model: urinary ureidopropanoate, for instance, was found to be negatively correlated with IL-12, IL-1 β and CXCL1 in the non-healing strain but did not correlate with cytokines in the self-healing model. In several instances, particularly in non-healing mice, metabolites that were correlated with IL-12, IL-1 β and or CXCL1 produced opposing or no correlative associations with regulatory cytokine IL-10. These disparate correlation patterns included 2-oxoisocaproate, PAG and lactate in the urine.

***Clostridia* and *Gammaproteobacteria* display opposing associations with host metabolites**

Extending further from the immune-metabolic correlations, associations between the host faecal microbiome and metabolism were similarly investigated, using percentage abundance of the different

bacterial classes and spectral NMR data as input parameters. Results for plasma and faeces have been summarised in Table 2 (Table S5 for urine). The majority of the metabolites that were negatively linked with the *Clostridia* class were positively linked to *Gammaproteobacteria* and *vice versa* in both mouse models. Such correlative metabolites included choline, glycerophosphocholine (GPC), plasma lipids, lactate, the gut-microbiota associated molecules hippurate, PAG and TMA, and metabolites related to the tricarboxylic acid cycle (e.g. acetate and fumarate) in the urine. *Erysipelotrichia* displayed similar correlation patterns with host urinary and faecal metabolites as *Clostridia* in both CL models, as well as with plasma metabolites in the self-healing C57BL/6 strain.

Multiple links between cytokines and faecal microbial classes in both infection models

Details of the correlation analyses between cytokine concentrations and microbial class abundances are summarised in Table 3. IL-1 β displayed the highest number of correlations with the microbiota in the self-healing phenotype. IL-1 β was found to be positively correlated with all microbial classes for at least one time-point in self-healing mice, yet was only correlated with *Bacilli* and *Gammaproteobacteria* in non-healing mice. IL-12 and IL-10 displayed the most immune-microbial correlations out of all the cytokines in the non-healing mice. *Actinobacteria* and *Bacteroidia* classes were strongly positively correlated with IL-10 levels in both strains, suggesting these commensal bacteria may exert IL-10 dependent anti-inflammatory effects on the host.

Differences in metabolic and microbial responses to *L. major* infection dominate separation between the self-healing and the non-healing phenotype

To ascertain the relative contribution of the host metabolic, immunological, and microbial backgrounds towards differentiating the two mouse strains' responses to *L. major* infection, metabolite integrals, cytokine concentrations, and bacterial percentage abundances were co-analysed by Partial

Least Squares discriminatory analyses (PLS-DA), shown in Figure 3. Average correlation of variances (CV's) for the selected metabolites across all post-infection time-points were 27.7% (urine), 39.2% (plasma) and 16.4% for BALB/C mice, and 32.8% (urine), 35.3% (plasma) and 20.5% for C57BL/6 mice. Analyses showed that metabolites in the urine and plasma represented the major drivers of separation between host responses of the two strains to infection, particularly at the beginning of infection, e.g. urinary hippurate and plasma glycine were found in higher concentrations in the self-healing phenotype (Figure 3). Hippurate remained consistently higher in this strain throughout the study, in addition to urinary creatine, faecal glutamate, and levels of the *Erysipelotrichia* and *Betaproteobacteria*. In contrast CXCL1, urinary PAG and plasma levels of 3-HB and lipid methyl groups were consistently higher in non-healing mice throughout infection. With infection progression, the faecal microbiota became the most discriminatory variables between the two strains. By the terminal time-point, members of the *Gammaproteobacteria* class were strongly linked with self-healing mice whilst *Clostridia* and *Bacilli* classes were associated with the non-healing phenotype (Figure 3).

Parasitic load associated with a select set of metabolic, immunological and microbial markers

In order to assess whether parasitic burden was linked to host metabolism, immune status and/or faecal microbiota, relative fluorescent intensities of lesion-derived *L. major* DNA were correlated with the same variables as used for the previous PLS-DA models (Figure 4). Faecal succinate and IL-12 were found to be positively linked with parasitic load in the self-healing mouse strain. In contrast, plasma scyllo-inositol, faecal acetate and *Betaproteobacteria* were positively associated with parasite counts in non-healing mice, whereas urinary 2-oxoisocaproate was negatively correlated.

***L. major* results in a CL model-specific systems response between host metabolism, immune system and microbiota**

Pair-wise Pearson correlation analysis was performed between selected variables to assess potential associations between the different host responses within each infection model. A separate model was built for each time-point and plotted as correlation network wheels, shown in Figure 5. The level of inter-connectivity between the variables differed between the two strains, even prior to infection, where the non-healing strain displayed hardly any correlations between variables (Figure S2). Infection resulted in a substantial increase in the number of correlative associations in the self-healing strain at d 2 p.i., the highest observed in this study, whereby each variable was directly correlated with at least one other variable. At d 6 p.i., non-healing mice displayed more associations between variables than earlier time-points, whilst correlations between variables in self-healing mice became more confined to their individual biological matrices. Multiple correlations were still observed in both models at the terminal time-point, whereby the two strains displayed many similarities in their correlation patterns.

Whilst the constrained format of the correlation wheels allows for direct comparisons of variables between strains or time-points, results were additionally depicted as network maps (Figures 6 and S3). The topology of the network maps is more conducive to interpretation than the correlation wheels, favouring the visualization of major hubs and chains of correlation within the networks, and thus more aligned with mapping to biological pathways. The maps demonstrated that metabolites in plasma and urine represented the core frameworks within the networks during the course of infection in both models, displaying the highest number of inter- and intra-matrix correlations. Acetate, citrate, and alanine represented major network hubs in the self-healing mouse model, with some of the highest numbers of direct associations across all three post-infection time-points. Unlike C57BL/6, network hubs in the non-healing strain were less stable through time and alternated throughout the course of the study, with only plasma lactate remaining highly correlated with other variables at the three post-infection time-points.

With the exception of d 2 p.i. in the BALB/c mice, IL-10 was consistently connected with multiple host components within the core network of both phenotypes, highlighting its systemic regulatory role within the host. The pro-inflammatory cytokine CXCL1 was directly correlated with numerous bacterial classes and metabolites across different biological matrices in both infected strains. IL-12 produced negligible correlations in the self-healing strain in the current study. Within the microbiota data, *Bacilli* and *Bacteroidia* classes were consistently disconnected from the core network hubs and were connected largely with themselves, if correlated at all. *Clostridia* and *Gammaproteobacteria* were negatively correlated with each other in both models across multiple time-points.

DISCUSSION

The current study presents a systematic characterisation of the global metabolic profile, peripheral cytokine status, and the faecal microbiome in both susceptible BALB/c and self-healing C57BL/6 mouse models of CL. The specific objective of the work was to reveal the immune–metabolic–microbial phenotype that underlies a successful response to *L. major*, using an integrated network approach. Within the immunological context of this study, the first assessed post-infection time-point (d 2 p.i.) represents an immune response that is entirely driven by innate factors. The two later time-points assessed (d 6 p.i. and terminal) are generally thought to be driven by the host's adaptive immunity.³² Whilst our study focused only on the early stages of disease, trends in increased lesion size and parasitic burden were already apparent in the non-healing model.

Key differences in strain-related metabolic responses towards infection included changes in glucose and lipid metabolism. The non-healing BALB/c mice appeared to rely predominantly on fatty acids rather than glucose as source of energy during infection, reflected by the relative increases in plasma glucose and 3-HB: a ketone body generated from fatty acid breakdown.³³ Biochemical blood results from the supplier indicate that BALB/c mice typically have nearly twice as much circulating triglycerides and lower levels of glucose in their blood than C57BL/6 mice.^{34, 35} This finding was in line with our results, where baseline plasma lipid moieties were also higher in BALB/c mice than in the C57BL/6 strain. However, *L. major* infection induced a pronounced decrease in lipids BALB/c mice only. It may thus be speculated that due to their high bioavailability, metabolism of fatty acids represents a major alternative for energy production in BALB/c mice not only in general but also more importantly in response to infection.

Alanine and succinate concentrations were found to be consistently higher across multiple biofluids (in faeces and for alanine, also in plasma) in the non-healing phenotype throughout infection. Both

metabolites represent major waste products of *Leishmania* species³⁶ and our results showed that succinate was also directly correlated with parasitic burden. Earlier *in vitro* studies have shown concentrations of alanine and succinate to be significantly higher in cell media from *L. major* infected macrophages when compared to uninfected macrophages³⁷, highlighting their potential role as biomarkers of *Leishmania* infection. It is thus plausible that these metabolites may in fact be directly derived from the parasite. Urinary hippurate levels decreased upon infection in both strains and, upon control-strain adjustment, were consistently found to be lower in the non-healing infected BALB/C mice when compared to the self-healing strain. Interestingly, a decrease in hippurate has also been observed in previous experimental rodent parasitic models (e.g. in *Trypanosoma brucei brucei* and *Schistosoma. mansoni* infections), indicating that this may be a more general marker of parasitic infection.^{16, 17}

Immunological investigation of the two infected strains confirmed the importance of the innate immune system driving the differential response during early stages of infection, whereby the non-healing model displayed an inherent pro-inflammatory phenotype compared with the self-healing strain. In contrast to published evidence³⁸, defining the role of Th1 cytokine IL-12 in the current study proved difficult, not only owing to the variable concentrations measured over the course of infection in both strains, but due to its observed positive association with parasitic load.

Following infection, marked changes in faecal bacterial composition were observed, most notably, the expression levels of members of the *Clostridia* class, which were higher in the non-healing strain, and *Gammaproteobacteria* classes, that were higher in self-healing mice. Our results indicate that the abundance of *Clostridia* and *Gammaproteobacteria* were inversely correlated, a finding that was also reported following weight-loss through bariatric surgery in rats by Li and colleagues.³⁹ In our study, the

two bacterial classes are often linked with the same metabolite but demonstrate contrasting directionality, a phenomenon that was apparent in both strains of mice.

Parasitic counts within the lesion of infected mice produced significant correlations with select biomarkers across the different responses assessed in this study. Twice as many correlates were observed in the non-healing mice. Plasma *scyllo*-inositol, an organic osmolyte that has recently been found to be associated brain disorders⁴⁰, represented the strongest associated variable with parasite counts in this strain.

Correlation network analyses between the host metabolic, cytokine, and faecal microbial responses during infection uniquely demonstrated direct statistical interactions between host components. Remarkable differences in the level of inter- and intra-matrix correlations were observed between the two strains and sampling time-points. The self-healing C57BL/6 strain displayed the maximal number of correlations between cytokines, microbiota, and metabolites 2 days after infection. Acetate, citrate and alanine represented major network hubs in the self-healing strain, implying that these metabolites may prove significant in orchestrating a systemic response towards *Leishmania*.

Acetate represents a key metabolite central to the metabolism of both carbohydrates and fatty acids, used predominantly for the formation of acetyl coenzyme A. Additionally, it is the main short-chain fatty acid readily reabsorbed from the colon back into systemic circulation and thus also acts as a marker of colonic fermentation of dietary carbohydrate.⁴¹ Both citrate (a tricarboxylic acid intermediate) and alanine (a gluconeogenic amino acid *via* the Cahill pathway⁴²) represent markers linked with host energy metabolism. Thus results from our study emphasise the focal role of carbohydrate metabolism within the self-healing model during infection, presumably to account for the high energy requirements to mount a successful system response towards the pathogen. In the non-healing mice, the highest number of associations between variables was observed 6 days post-infection,

with few correlations observed at earlier time-points. The associations in the non-healing phenotype appeared to be connected at random (disordered) rather than as functionally structured hubs, as in self-healing mice. It could thus be hypothesised that these highly connected interactions between multiple compartments within the host are vital for mounting a rapid and effective innate immune response towards *L. major*, as seen in the self-healing state.

CONCLUSIONS

In summary, our systemic approach to the characterisation of two experimental models of a *L. major* infection adds a novel aspect to the assessment of host defence, which can be applied to other disease models. Tangible differences between the infection models included differences in energy metabolism, inflammatory status, and gut microbial composition. Furthermore, our study revealed parasitic-linked metabolites that were higher in the non-healing model and provide novel candidates to be further investigated as potential biomarkers of *Leishmania* infection. Globally we have shown that already during the innate immune response, an efficiently orchestrated network of metabolic, immunological, and gut microbial features may be linked to a successful pathogen defence. Infection in the self-healing model displayed a comprehensive correlation network between multiple biological responses towards the parasite that was not present in the non-healing model, which may explain the superiority of this strain in controlling disease. We have also identified a suite of metabolic candidates that represented major network hubs linked to a successful immune response to *L. major*, which can be further explored to ascertain potential indices for immune-modulatory and/or leishmanicidal activity.

ASSOCIATED CONTENT

Supporting Information

This section contains three figures and five tables and supporting protocols, titles listed below. This material is available free of charge *via* the Internet at <http://pubs.acs.org>.

- Figure S1. *L. major* infection-related changes in cytokine levels in plasma from two CL models
- Figure S2. Statistical inter-connectivity of metabolic, immune, and microbial markers in mouse models prior to infection
- Figure S3. Correlation network map of metabolic, immune and microbial markers of CL models (Terminal day)
- Table S1. Physiological and pathological measures of CL mouse models
- Table S2. Infection-related discriminatory metabolic markers between the two CL models
- Table S3. Infection-related differences in faecal microbiotal composition between the two CL models
- Table S4. Infection-related differences in faecal microbiotal composition over time within each CL model
- Table S5. Microbial-metabolic correlates in urine of CL models
- Supporting Protocols

AUTHOR INFORMATION

Corresponding author

* E-mail: jasmina.saric@imperial.ac.uk

Author Contributions

JS, KS, SC and EH conceived and designed the study. Animal handling and sample collection were performed by JS. Sample preparation, acquisition and analyses were performed by SDL. EG and SDL performed parasitic burden assessment, under the supervision and guidance of MER. Faecal microbial DNA extraction and PCR were performed by SDL, under the supervision and guidance of JRM. KAV and JMP provided statistical guidance and analytical MATLAB codes for correlation analyses. SDL, JS and EH wrote the manuscript, including critical input and final approval from all authors.

Notes

The authors declare that they have no competing interests.

ACKNOWLEDGMENTS

We would like to thank the Wellcome Trust for financial support of the research presented in the current manuscript (Sir Henry Wellcome Fellowship JS, Award number 089002/B/09/Z) and the MRC and Imperial College for the MRC Doctoral Training Award for SDL's studentship funds. KAV acknowledges the junior research fellowship scheme by Imperial College London. We would like to thank The Royal Society for funding the compute cluster HIVE at Cardiff University and the Biotechnology and Biological Sciences Research Council for support for MER and EG (David Phillips Fellowship MER, Award number BB/H022406/1). The funding bodies had no role in study design, data collection and analysis, decision to publish, or preparation of the manuscript.

ABBREVIATIONS

CL, Cutaneous Leishmaniasis; CXCL, chemokine (C-X-C motif) ligand; DALY, disability-adjusted life year; IL, Interleukin; PCR, polymerase chain reaction; Th, T helper cell.

REFERENCES

1. Desjeux, P. *Nat Rev Micro* **2004**, *9*, 692-693.
2. Alvar, J.; Velez, I. D.; Bern, C.; Herrero, M.; Desjeux, P.; Cano, J.; Jannin, J.; den Boer, M.; WHO Leishmaniasis Control Team *PLoS One* **2012**, *5*, e35671.
3. Croft, S. L.; Olliaro, P. *Clin. Microbiol. Infect.* **2011**, *10*, 1478-1483.
4. Scott, P. J. *J. Immunol* **1991**, *9*, 3149-3155.
5. Sypek, J. P.; Chung, C. L.; Mayor, S. E.; Subramanyam, J. M.; Goldman, S. J.; Sieburth, D. S.; Wolf, S. F.; Schaub, R. G. *J. Exp. Med.* **1993**, *6*, 1797-1802.
6. Sadick, M. D.; Heinzl, F. P.; Holaday, B. J.; Pu, R. T.; Dawkins, R. S.; Locksley, R. M. *J. Exp. Med.* **1990**, *1*, 115-127.
7. Kopf, M.; Brombacher, F.; Köhler, G.; Kienzle, G.; Widmann, K. H.; Lefrang, K.; Humborg, C.; Ledermann, B.; Solbach, W. *J. Exp. Med.* **1996**, *3*, 1127-1136.
8. Belkaid, Y.; Piccirillo, C. A.; Mendez, S.; Shevach, E. M.; Sacks, D. L. *Nature* **2002**, *6915*, 502-507.
9. Woelbing, F.; Kostka, S. L.; Moelle, K.; Belkaid, Y.; Sunderkoetter, C.; Verbeek, S.; Waisman, A.; Nigg, A. P.; Knop, J.; Udey, M. C.; von Stebut, E. *J. Exp. Med.* **2006**, *1*, 177-188.
10. Peters, N. C.; Egen, J. G.; Secundino, N.; Debrabant, A.; Kimblin, N.; Kamhawi, S.; Lawyer, P.; Fay, M. P.; Germain, R. N.; Sacks, D. *Science* **2008**, *5891*, 970-974.

11. Iniesta, V.; Carcelen, J.; Molano, I.; Peixoto, P. M. V.; Redondo, E.; Parra, P.; Mangas, M.; Monroy, I.; Campo, M. L.; Gomez Nieto, C.; Corraliza, I. *Infect. Immun.* **2005**, *9*, 6085-6090.
12. Kropf, P.; Fuentes, J. M.; Fahrnich, E.; Arpa, L.; Herath, S.; Weber, V.; Soler, G.; Celada, A.; Modolell, M.; Muller, I. *FASEB Journal* **2005**, *8*, 1000-1002.
13. Li, P.; Yin, Y.; Li, D.; Woo Kim, S.; Wu, G. *Br. J. Nutr.* **2007**, *02*, 237-252.
14. Saric, J. *Parasitology* **2010**, *Special Issue 09*, 1451.
15. Ferrante Jr, A. W. *J. Clin. Invest.* **2013**, *12*, 4992-4993.
16. Wang, Y.; Holmes, E.; Nicholson, J. K.; Cloarec, O.; Chollet, J.; Tanner, M.; Singer, B. H.; Utzinger, J. *Proc. Natl. Acad. Sci. U. S. A.* **2004**, *34*, 12676-12681.
17. Wang, Y.; Utzinger, J.; Saric, J.; Li, J. V.; Burckhardt, J.; Dirnhofer, S.; Nicholson, J. K.; Singer, B. H.; Brun, R.; Holmes, E. *Proc. Natl. Acad. Sci. U. S. A.* **2008**, *16*, 6127-6132.
18. Dumas, M.; Maibaum, E. C.; Teague, C.; Ueshima, H.; Zhou, B.; Lindon, J. C.; Nicholson, J. K.; Stamler, J.; Elliott, P.; Chan, Q.; Holmes, E. *Anal. Chem.* **2006**, *7*, 2199-2208.
19. Schreier, C.; Kremer, W.; Huber, F.; Neumann, S.; Pagel, P.; Lienemann, K.; Pestel, S. *Biomed. Res. Int.* **2013**, , 878374.
20. Saric, J.; Li, J. V.; Swann, J. R.; Utzinger, J.; Calvert, G.; Nicholson, J. K.; Dirnhofer, S.; Dallman, M. J.; Bictash, M.; Holmes, E. *J. Proteome Res.* **2010**, *5*, 2255-2264.
21. Saric, J.; Li, J. V.; Wang, Y.; Keiser, J.; Bundy, J. G.; Holmes, E.; Utzinger, J. *PLoS Negl. Trop. Dis.* **2008**, *7*, e254.

22. Oliveira, M. R.; Tafuri, W. L.; Afonso, L. C.; Oliveira, M. A.; Nicoli, J. R.; Vieira, E. C.; Scott, P.; Melo, M. N.; Vieira, L. Q. *Parasitology* **2005**, *4*, 477-488.
23. Beckonert, O.; Keun, H. C.; Ebbels, T. M.; Bundy, J.; Holmes, E.; Lindon, J. C.; Nicholson, J. K. *Nat. Protoc* **2007**, *11*, 2692-2703.
24. Dieterle, F.; Ross, A.; Schlotterbeck, G.; Senn, H. *Anal. Chem.* **2006**, *13*, 4281-4290.
25. Lewis, D. A.; Brown, R.; Williams, J.; White, P.; Jacobson, S. K.; Marchesi, J.; Drake, M. J. *Front. Cell. Infect. Microbiol.* **2013**, *41*,.
26. de La Llave, E.; Lecoecur, H.; Besse, A.; Milon, G.; Prina, E.; Lang, T. *Cell. Microbiol.* **2011**, *1*, 81-91.
27. Solcà, M. d. S.; Guedes, C. E. S.; Nascimento, E. G.; Oliveira, G. G. d. S.; Santos, W. L. C. d.; Fraga, D. B. M.; Veras, P. S. T. *Vet. Parasitol.* **2012**, *2-4*, 133-140.
28. Hotelling, H. *J. Educ. Psychol.* **1933**, *6*, 417.
29. Trygg, J.; Holmes, E.; Lundstedt, T. *J. Proteome Res.* **2007**, *2*, 469-479.
30. Poma, J. M.; Robinette, S. L.; Holmes, E.; Nicholson, J. K. *Bioinformatics* **2013**, .
31. Storey, J. D.; Tibshirani, R. *PNAS* **2003**, *16*, 9440-9445.
32. Janeway, C. A. J.; Travers, P.; Walport, M.; Shlomchik, M. J. Principles of innate and adaptive immunity. In *Immunobiology: The Immune System in Health and Disease*; Garland Science: New York, 2001; .

33. Morris, A. A. M. *J. Inherit. Metab. Dis.* **2005**, *2*, 109-121.
34. Charles River Laboratories Clinical Pathology Data for BALB/c Mouse Colonies in North America for January 2008 - December 2012. http://www.criver.com/files/pdfs/rms/balbc/rm_rm_r_balbc_mouse_clinical_pathology_data.aspx (accessed August 5, 2014).
35. Charles River Laboratories Biochemistry and Hematology for C57BL/6NCrI Mouse Colonies in North American for January 2008 – December 2012. http://www.criver.com/files/pdfs/rms/c57bl6/rm_rm_r_c57bl6_mouse_clinical_pathology_data.aspx (accessed August 5, 2014).
36. McConville, M. J.; de Souza, D.; Saunders, E.; Likic, V. A.; Naderer, T. *Trends Parasitol.* **2007**, *8*, 368-375.
37. Lamour, S. D.; Choi, B.; Keun, H. C.; Müller, I.; Saric, J. *J. Proteome Res.* **2012**, *8*, 4211-4222.
38. Sacks, D.; Noben-Trauth, N. *Nat. Rev. Immunol.* **2002**, *11*, 845.
39. Li, J. V.; Ashrafian, H.; Bueter, M.; Kinross, J.; Sands, C.; le Roux, C. W.; Bloom, S. R.; Darzi, A.; Athanasiou, T.; Marchesi, J. R.; Nicholson, J. K.; Holmes, E. *Gut* **2011**, *9*, 1214-1223.
40. Griffith, H. R.; den Hollander, J. A.; Stewart, C. C.; Evanochko, W. T.; Buchthal, S. D.; Harrell, L. E.; Zamrini, E. Y.; Brockington, J. C.; Marson, D. C. *NMR Biomed.* **2007**, *8*, 709-716.
41. Hijova, E.; Chmelarova, A. *Bratisl. Lek. Listy* **2007**, *8*, 354-358.
42. Felig, P.; Pozefsk, T.; Marlis, E.; Cahill, G. F. *Science* **1970**, *3920*, 1003-1004.

FIGURES

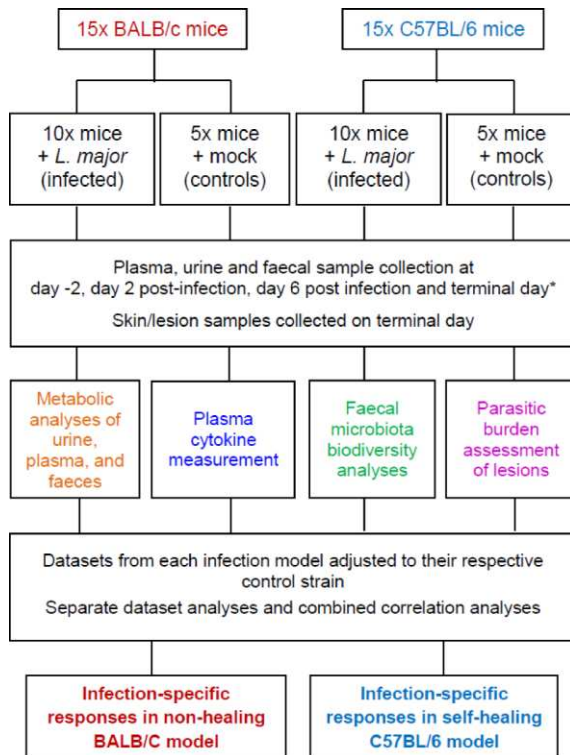


Figure 1. Schematic overview of study

Study compares experimental cutaneous leishmaniasis in non-healing BALB/c mice versus self-healing C57BL/6 mice, during early phases of *L. major* infection (see Materials and Methods). *Terminal day defined for each infected mouse on the day shortly before lesion ulceration (days 7-13) or on day 12 for control mice.

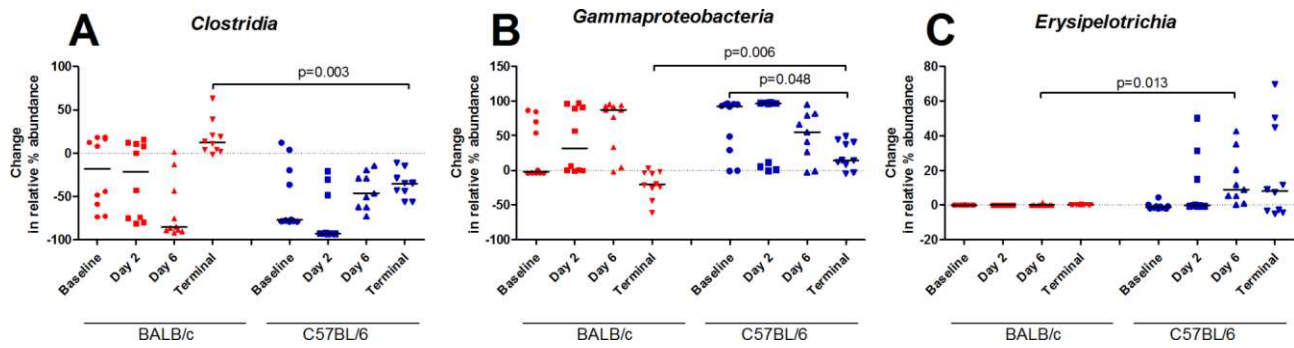


Figure 2. Changes in faecal microbial composition between the two mouse CL models

Infection-related changes in composition of the bacterial classes *Clostridia* (A), *Gammaproteobacteria* (B) and *Erysipelotrichia* (C) in faeces of infected mice, adjusted to their respective control strain. Horizontal bars represent group median averages and each symbol represents a faecal sample ($n=10$ for all groups except C57BL/6 Day 6 where $n=9$).

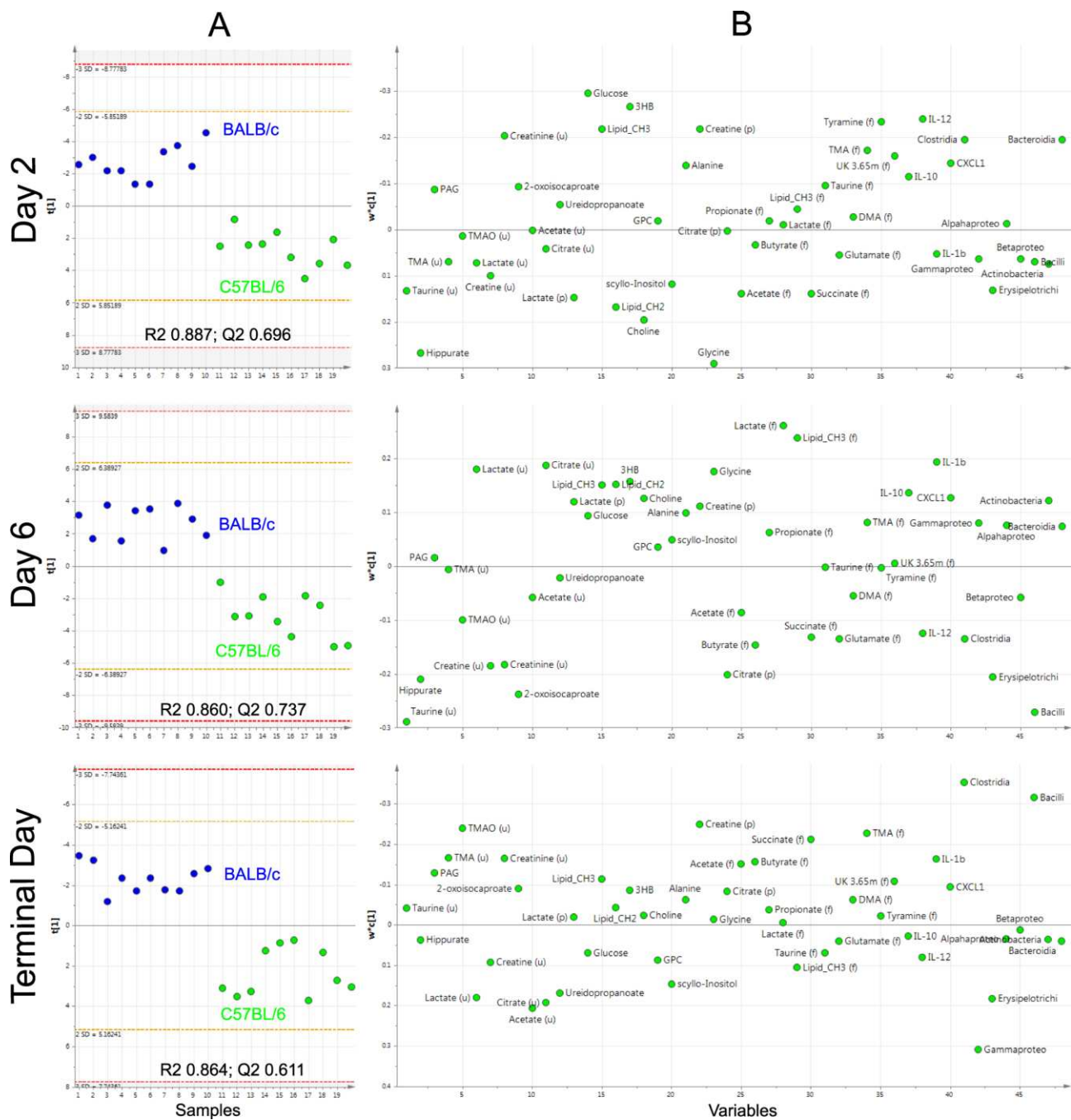


Figure 3. Discriminatory variables between two infection models for each post-infection time-point assessed via PLS-DA

Scores plots (A) and corresponding loadings plots (B) of Partial Least Squares discriminatory analyses (PLS-DA) between the two infected strains are presented, based on the first component vector for 2 days and 6 days post-infection and at the terminal study day. A) Each circle represents one sample.

BALB/c (blue) and C57BL/6 (green) samples are separated into the two infection models, vertically along the first PLS vector $t[1]$. Horizontal hashed lines represented two and three standard deviations (SD) from the mean. B) Relative contribution of each of the discriminatory variables (circles) towards the vertical mouse model separation in the associated scores plot, composed of 48 markers in the following order: 12 urinary (u), 12 plasma (p), and 12 faecal metabolites (f), four cytokines, and eight percentage abundance of eight microbial classes. Origin of metabolites present in more than biofluid additionally labelled with (u), (p) or (f). R2 and Q2 describe fit and predictive value of each model, respectively. Key: 3HB, 3-hydroxybutyrate; GPC, glycerophosphocholine; PAG, pheynylacetyl glycine; TMA, trimethylamine; TMAO, trimethylamine-N-oxide; UK 3.65m, unassigned multiplet at δ 3.65.

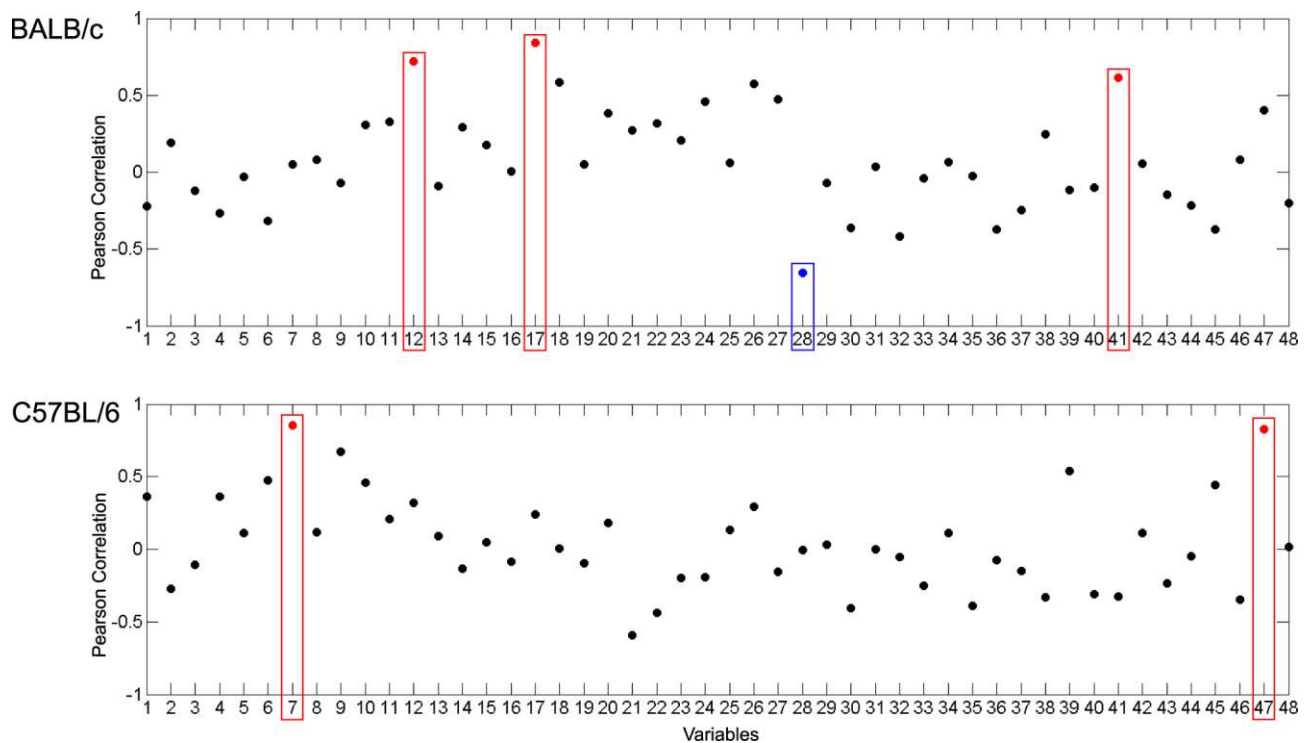


Figure 4. Correlation between parasitic burden and host response markers in non-healing and self-healing CL models

Plot shows Pearson correlation between relative amount of *L. major* DNA in lesions (Table S1) from infected BALB/c and C57BL/6 mice, and levels of infection-related metabolic, immune and faecal microbial variables (terminal time-point). Each variable is represented by a small circle, where significantly positively correlated variables are boxed in red and negative in blue ($q < 0.3$). Key: faecal metabolites; 1, unassigned multiplet peak at δ 3.65; 2, tyramine; 3, trimethylamine (TMA); 4, dimethylamine; 5, glutamate; 6, taurine; 7, succinate; 8, lipid (CH3); 9, lactate; 10, propionate; 11, butyrate; 12, acetate. Plasma metabolites; 13, citrate; 14, glycine; 15, creatine; 16, alanine; 17, scyllo-inositol; 18, glycerophosphocholine; 19, choline; 20, 3-hydroxybutyrate; 21, lipid (CH2); 22, lipid (CH3); 23, glucose; 24, lactate. Urine metabolites; 25, ureidopropanoate; 26, citrate; 27, acetate; 28, 2-oxoisocaproate; 29, creatinine; 30, creatine; 31, lactate; 32, trimethylamine-N-oxide; 33, TMA; 34,

phenylacetylglycine; 35, hippurate; 36, taurine. Bacterial classes; 37, *Clostridia*; 38, *Gammaproteobacteria*; 39, *Erysipelotrichia*; 40, *Alphaproteobacteria*; 41, *Betaproteobacteria*; 42, *Bacilli*; 43, *Actinobacteria*; 44, *Bacteroidia*. Cytokines; 45, CXCL1; 46, IL-1 β ; 47, IL-12; 48, IL-10.

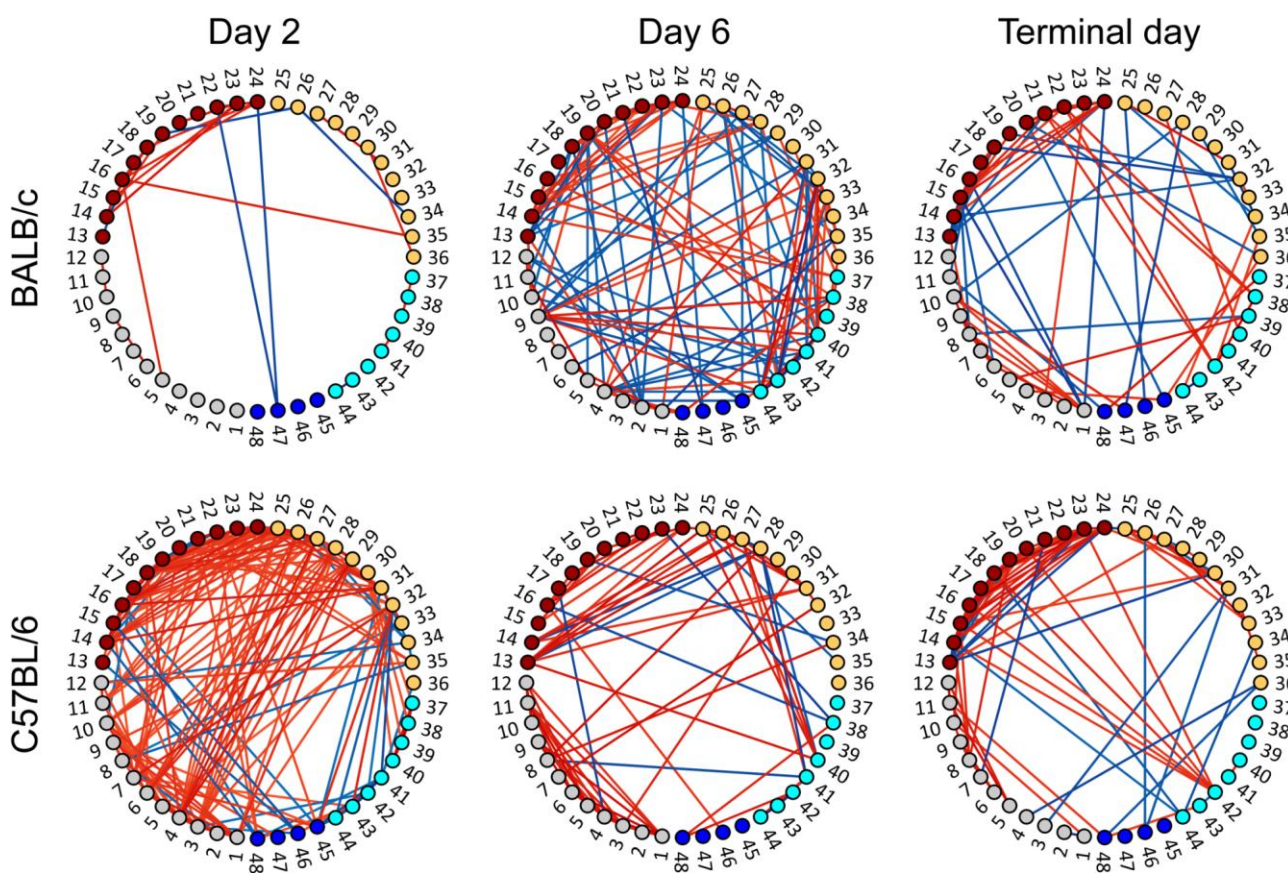


Figure 5. Correlation wheels of metabolic, immune, and microbial markers during acute infection in two CL models

Correlation networks for each measured time-point post-infection based on pair-wise Pearson correlation between selected variables for *L. major* infected BALB/c and C57BL/6 mice (see Figure S3 for pre-infection results). Red and blue connecting lines between variables represent significant positive and negative correlations, respectively ($q < 0.3$). The structure of the wheels is constrained such that variables have a fixed position and have colour-coded nodes along the circumference. Key: Grey, faecal metabolites; 1, unassigned multiplet peak at 3.65 ppm; 2, tyramine; 3, trimethylamine (TMA); 4, dimethylamine; 5, glutamate; 6, taurine; 7, succinate; 8, lipid (CH₃); 9, lactate; 10, propionate; 11, butyrate; 12, acetate. Red, plasma metabolites; 13, citrate; 14, glycine; 15, creatine; 16, alanine; 17, scyllo-inositol; 18, glycerophosphocholine; 19, choline; 20, 3-hydroxybutyrate; 21, lipid (CH₂); 22,

lipid (CH3); 23, glucose; 24, lactate. Yellow, urine metabolites; 25, ureidopropanoate; 26, citrate; 27, acetate; 28, 2-oxoisocaproate; 29, creatinine; 30, creatine; 31, lactate; 32, trimethylamine-N-oxide; 33, TMA; 34, phenylacetyl glycine; 35, hippurate; 36, taurine. Cyan, bacterial classes; 37, *Clostridia*; 38, *Gammaproteobacteria*; 39, *Erysipelotrichia*; 40, *Alphaproteobacteria*; 41, *Betaproteobacteria*; 42, *Bacilli*; 43, *Actinobacteria*; 44, *Bacteroidia*. Dark blue, cytokines; 45, CXCL1; 46, IL-1 β ; 47, IL-12; 48, IL-10.

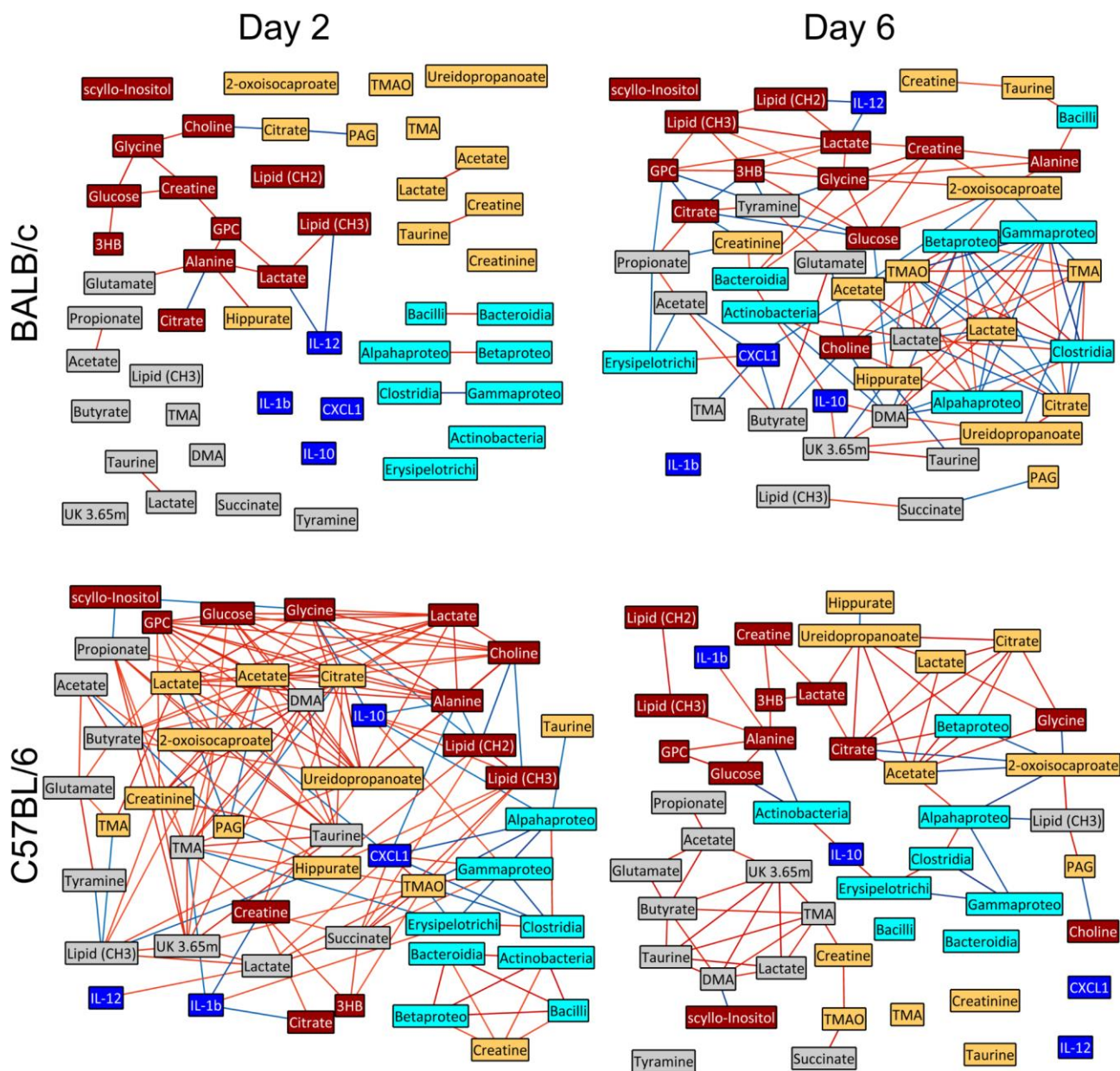


Figure 6. Correlation network map of metabolic, immunologic and microbial markers in response to early infection in two mouse CL models

Correlation networks based on pair-wise Pearson correlation between all variables for BALB/c and C57BL/6 mice infected with *L. major*, at 2 and 6 days post-infection (see Figure S3 for terminal). Red and blue connecting lines between variables represent significant positive or negative correlations, respectively ($q < 0.3$). Variables are grouped according to correlation clusters and are colour coded in

boxes according to their compartments: urine in yellow, plasma in red, cytokines in dark blue and bacterial classes in cyan. Key: 3HB, 3-hydroxybutyrate; DMA, dimethylamine; GPC, glycerophosphocholine; PAG, phenylacetyl glycine; TMA, trimethylamine; TMAO, trimethylamine-N-oxide; UK 3.65m, unassigned multiplet peak at δ 3.65.

TABLES

Table 1. Immune–metabolic correlates in urine, plasma, and faeces of the self-healing and non-healing CL infection models

Biofluid	Metabolite Correlate	Infected BALB/c				Infected C57BL/6			
		IL-10	IL-12	IL-1β	CXCL1	IL-10	IL-12	IL-1β	CXCL1
Urine	2-oxoadipate*					-		-	
	2-oxoglutarate							-	
	2-oxoisocaproate	+	-	-	-		+		
	Acetate				-	-			
	<i>cis</i> -Aconitate			-					
	Citrate		-				+		+
	Creatine				-	+/-			+
	Creatinine			-					
	Fumarate				-				
	Guanidoacetate		-		+				
	Hippurate	-	-			-			
	Lactate	+	-	-		-		-	
	PAG		+		+/-		+	+	+
	Succinate				-			-	
	Taurine	-	-		+/-	+/-	-	+	+
	TMA							-	-
	TMAO					+	+		+/-
Ureidopropanoate		-	-	-					
Plasma	β-HB								+
	Choline		+						
	Glucose	+	+		-	+/-		+	+/-
	Glycine					-			
	GPC		-						
	Lactate	+/-	-	-				+	
	Lipid CH ₂		-			+			+
	Lipid CH ₃		-			+			+
	Lipid* 3.22(m)					+			+
	<i>scyllo</i> -Inositol*			-					
Faeces	Butyrate		-		-	+			
	Glutamate						-		
	Lactate						+		+/-
	Lipid CH ₃						+		
	Propionate		+				+		+
	Succinate							-	+
	Taurine						+		

Key: +, positive correlations; -, negative correlations; +/-, direction of correlation alternated between different time-points; *, tentative assignment; 3-HB, 3-hydroxybutyrate; GPC, glycerophosphocholine; (m), unassigned multiplet (accompanied by chemical shift region); PAG, phenylacetyl glycine; TMA, trimethylamine; TMAO; trimethylamine-N-oxide.

Table 2. Microbial–metabolic correlates in plasma and faeces in the self-healing and non-healing infection models

Biofluid	Metabolic Correlate	Clos	Gamma	Erysi	Alpha	Beta	Bacil	Actino	Bacter
BALB/c: Plasma	3-HB			+	+			+	
	Choline	+	-	+	+			+	+
	Glucose	-		+	--	-	+	-	+
	GPC	-	+	+	-	-			-
	Lactate				+/-		-	-	
	Lipid* 3.22(m)			+	-			+	
	Lipid CH ₂		+	+	+/-	-		+	
	Lipid CH ₃			+	+/-	-		+	
	s-Inositol*				-	+/-		+	-
BALB/c: Faeces	Acetate			-					
	Butyrate	-	+	-		+	+		-
	Lactate						-		
	Propionate		+	-			-		
	Succinate						-		
C57BL/6: Plasma	3-HB	-	+	-	-				
	Choline	-	+						
	Glucose			-	-			--	++
	GPC	-	+						
	Lactate	-						-	
	Lipid* 3.22(m)	-	+	-					
	Lipid CH ₂	-	+	-					
	Lipid CH ₃	-		-					
C57BL/6:	Acetate					+	+	-	
	Butyrate							-	

Faeces	DMA			-					
	Glutamate			-			-		
	Lactate	-	+	-	-				+
	Propionate	-	+					-	
	Succinate	-	+	-	-				

Key: +, positive correlations at one time-point; ++ positive correlations for at least two time-points; -, negative correlations at one time-point; --; negative correlation for at least two time-points; +/-, direction of correlation alternating between different time-points; *, tentative assignment; 3.22(m), multiplet spectral peak at δ 3.22; 3-HB, 3-hydroxybutyrate; Actino, *Actinobacteria*; Alpha, *Alphaproteobacteria*; Bacil, *Bacilli*; Bacter, *Bacteroidia*; Beta, *Betaproteobacteria*; Clos, *Clostridia*; DMA; dimethylamine; Erysi, *Erysipelotrichia*; Gamma, *Gammaproteobacteria*; GPC, glycerophosphocholine; (m), unassigned multiplet (accompanied by chemical shift region); PAG, phenylacetyl glycine; *s-*, *scyllo*.

Table 3. Immune–microbial correlates across the self-healing and non-healing infection models

Microbial Class	Infected BALB/c				Infected C57BL/6			
	IL-10	IL-12	IL-1 β	CXCL 1	IL-10	IL-12	IL-1 β	CXCL 1
<i>Clostridia</i>	+	++				+	++	
<i>Gammaproteobacteria</i>			+/-	+	+		+	+
<i>Erysipelotrichia</i>		+		++	+	+	+	
<i>Alphaproteobacteria</i>	++	+				+	++	
<i>Betaproteobacteria</i>	+/-					+	++	
<i>Bacilli</i>		+	+		+	+	+	
<i>Actinobacteria</i>	++	+			++		+	
<i>Bacteroidia</i>	++	+			+	+	+	

Key: +, positive correlations at one time-point; ++ positive correlations for at least two time-points;
+/-, direction of correlation alternating between different time-points.

ABSTRACT GRAPHIC

Correlation networks show enhanced systems response in self-healing model post *Leishmania major* infection

